Beyond the "Spine of Hydration": Chiral SFG Spectroscopy Detects DNA First Hydration Shell and Base Pair Structures

Ethan A. Perets[1#†], Daniel Konstantinovsky[1,2§†], Ty Santiago[1], Pablo E. Videla[1ᵡ], Matthew Tremblay[1], Luis Velarde[3], Victor S. Batista[1], Sharon Hammes-Schiffer[1,4]*, E. C. Y. Yan[1]*

[1]Department of Chemistry, Yale University, New Haven, CT 06520, USA

[2]Department of Molecular Biophysics and Biochemistry, Yale University, New Haven, CT 06520, USA

[3]Department of Chemistry, University at Buffalo, State University of New York, Buffalo, NY 14260, USA

[4]Department of Chemistry, Princeton University, Princeton, NJ 08544, USA

[#]Current Address: Department of Molecular Biology, University of Texas Southwestern Medical Center, Dallas, TX 75390, USA

[§]Current Address: Department of Chemistry, Columbia University, New York, NY 10027, USA

[ᵡ]Current Address: Schrödinger, LLC, New York, NY 10036, USA

[†]Equal Contribution

*Corresponding Authors

Abstract

Experimental methods capable of selectively probing water at the DNA minor groove, major groove, and phosphate backbone are crucial for understanding how hydration influences DNA structure and function. Chiral-selective sum frequency generation spectroscopy (chiral SFG) is unique among vibrational spectroscopies because it can selectively probe water molecules that form chiral hydration structures around biomolecules. However, interpreting chiral SFG spectra is challenging since both water and the biomolecule can produce chiral SFG signals. Here, we combine experiment and computation to establish a theoretical framework for rigorous interpretation of chiral SFG spectra of DNA. We demonstrate that chiral SFG detects the N-H stretch of DNA base pairs and the O-H stretch of water, exclusively probing water molecules in the DNA first hydration shell. Our analysis reveals that DNA transfers chirality to water molecules only within the first hydration shell, so they can be probed by chiral SFG spectroscopy. Beyond the first hydration shell, electric field-induced water structure is symmetric and therefore precludes chiral SFG response. Furthermore, we find that chiral SFG can differentiate chiral subpopulations of first hydration shell water molecules at the minor groove, major groove, and phosphate backbone. Our findings challenge the scientific perspective dominant for more than 40 years that the minor groove "spine of hydration" is the only chiral water structure surrounding the DNA double helix. By identifying the molecular origins of the DNA chiral SFG spectrum, we lay a robust experimental and theoretical foundation for applying chiral SFG to explore the chemical and biological physics of DNA hydration.

Introduction

Watson and Crick recognized that DNA secondary structure is a function of hydration content.[1] The "rather high" water content around DNA to which the scientists alluded was later elucidated by the discovery of a chiral helix of water molecules in the DNA minor groove.[2-6] This "spine of hydration" comprises approximately 2 water molecules per base pair[3] of double-stranded DNA (dsDNA) and accounts for around 3-6% of the first hydration shell.[7] Despite ample structural evidence for the spine of hydration, other water structures around dsDNA have eluded experimental characterization. Methods capable of probing dsDNA hydration structures beyond the spine of hydration promise deeper understanding of how water influences dsDNA structure and determines the specificity of molecular binding and chemical reactivity. In this study, we combine experimental and theoretical approaches using chiral-selective vibrational sum frequency generation (chiral SFG) spectroscopy and provide a rigorous interpretation of the chiral SFG spectrum of dsDNA hydration structures.

Vibrational spectroscopies, such as Raman,[8, 9] ultrafast two-dimensional infrared,[10] and terahertz spectroscopies,[11] offer sensitive, label-free approaches to probing hydration structures. Vibrational spectroscopies can distinguish dsDNA hydration shell water molecules by non-bulk-like water dynamics[11-14] or by distinct molecular interactions, for example, unique hydrogen-bonding structures compared to bulk water.[15, 16] Alternatively, native molecular probes, such as the negatively-charged phosphate groups of dsDNA, offer indirect readouts of hydration shell water structures and dynamics.[10, 17] However, vibrational spectroscopies may fail to detect dsDNA hydration shell structures when the interactions or dynamics of water molecules in hydration shells are too similar to bulk water.

Recently, it has been recognized that chiral SFG can detect hydration structures around DNA and protein.[6, 18-22] Chiral SFG is sensitive to the macroscopic chirality of biomacromolecules, such as protein secondary structures[23-26] and dsDNA[27, 28] as well as chiral assemblies of achiral molecules.[25, 29-31] Because water molecules are achiral, chiral SFG only detects chiral assemblies of multiple water molecules, such as the spine of hydration. Petersen and co-workers first reported chiral SFG vibrational signatures of O-H

stretching of water around dsDNA.[6] They assigned the vibrational response to water molecules in the spine of hydration and attributed sequence-dependent effects in the chiral SFG spectra to sequence-dependent water structures within the dsDNA minor groove. Their pioneering study suggested that chiral SFG has high sensitivity and specificity for water molecules within the dsDNA hydration shell, which prompts two major questions. Can chiral SFG probe hydration structures beyond the minor groove spine of hydration, and detect water structures hydrating the major groove and phosphate backbone of DNA? What are the contributions of nucleotide vibrations in the chiral SFG response? Answering these questions is paramount for providing an accurate molecular interpretation of chiral SFG spectra of DNA.

In this report, we address these two key questions using tandem experimental and computational chiral SFG approaches, akin to those developed in our previous studies of protein hydration.[19, 20, 22, 28, 32, 33] We identify chiral SFG vibrational signatures from the O-H stretching of water molecules that form chiral hydration structures around $(dA)_{12} \cdot (dT)_{12}$ dsDNA, as well as stretching modes of adenine NH_2, which forms hydrogen bonds in canonical adenine-thymine basepairs. Using native (D-) and non-native (L-) dsDNA enantiomers, we confirm that the handedness of the dsDNA double helix templates the handedness of chiral hydration structures around dsDNA. Overall, we demonstrate that N-H stretching of dsDNA, as well as O-H stretching of water molecules hydrating not only the minor groove but also the major groove and the phosphate backbone, can contribute to the chiral SFG response. Our results establish that chiral SFG is sensitive to dsDNA nucleotide vibrations as well as to hydration structures beyond the minor groove spine of hydration.[6] We conclude that chiral SFG is exclusively sensitive to the structure of the dsDNA first hydration shell. The ability of chiral SFG to study the structure of the first hydration shell around dsDNA will help answer important questions in DNA biology, including the role of water in DNA biomolecular recognition, chromatin remodeling, epigenetic modification, and genetic regulation.

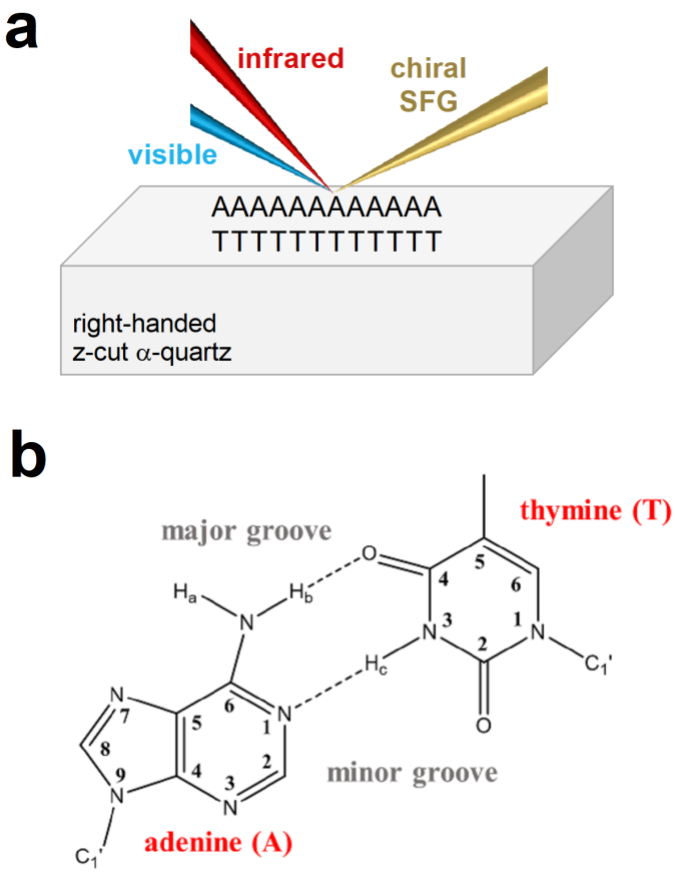

Figure 1. (a) Schematic of chiral SFG spectroscopy of $(dA)_{12} \cdot (dT)_{12}$ dsDNA hydrated films dropcast at the air-quartz interface. Chiral-sensitive *psp* polarization is achieved by detecting the *p*-polarized chiral SFG output with *s*-polarized visible and *p*-polarized infrared input laser beams (see Methods). (b) Adenine-thymine base pairs showing minor groove and major groove chemical moieties.

Results

Chiral SFG reveals vibrational resonances due to water O-H and dsDNA N-H.

We implement phase-resolved heterodyne chiral SFG for the study of dsDNA hydration (see Methods). In our experiments, hydrated films of $(dA)_{12} \cdot (dT)_{12}$ dsDNA are dropcast on a right-handed z-cut α-quartz crystal substrate under ambient conditions and probed by ultrafast pulsed infrared and visible lasers (Figure 1a). Overlapping the linearly polarized infrared and visible pulses in time and space at the sample surface enables detection of the chiral SFG response of water and dsDNA (Figure 2a, top panel). We begin by assigning vibrational features in the experimental chiral SFG spectrum of $(dA)_{12} \cdot (dT)_{12}$

dsDNA in the region of 2960-3800 cm^{-1}. Chiral SFG vibrations from 2960-3100 cm^{-1} likely arise from C-H stretching modes of adenine, thymine, and/or the DNA sugar.[28, 34] For $(dA)_{12} \cdot (dT)_{12}$ dsDNA, vibrational resonances above 3200 cm^{-1} can arise from adenine base NH_aH_b stretching (Figure 1b) or water O-H stretching modes. Previous studies did not attribute N-H contribution in the chiral SFG spectra of $(dAdT)_{12} \cdot (dAdT)_{12}$ dsDNA.[6] However, N-H and O-H vibrations can be experimentally distinguished by $H_2{}^{18}O$ isotopic substitution. Substitution with $H_2{}^{18}O$ is expected to red-shift vibrational bands originating from the O-H stretching modes of water.[19, 20, 35] Vibrational resonances due to dsDNA should not red-shift.

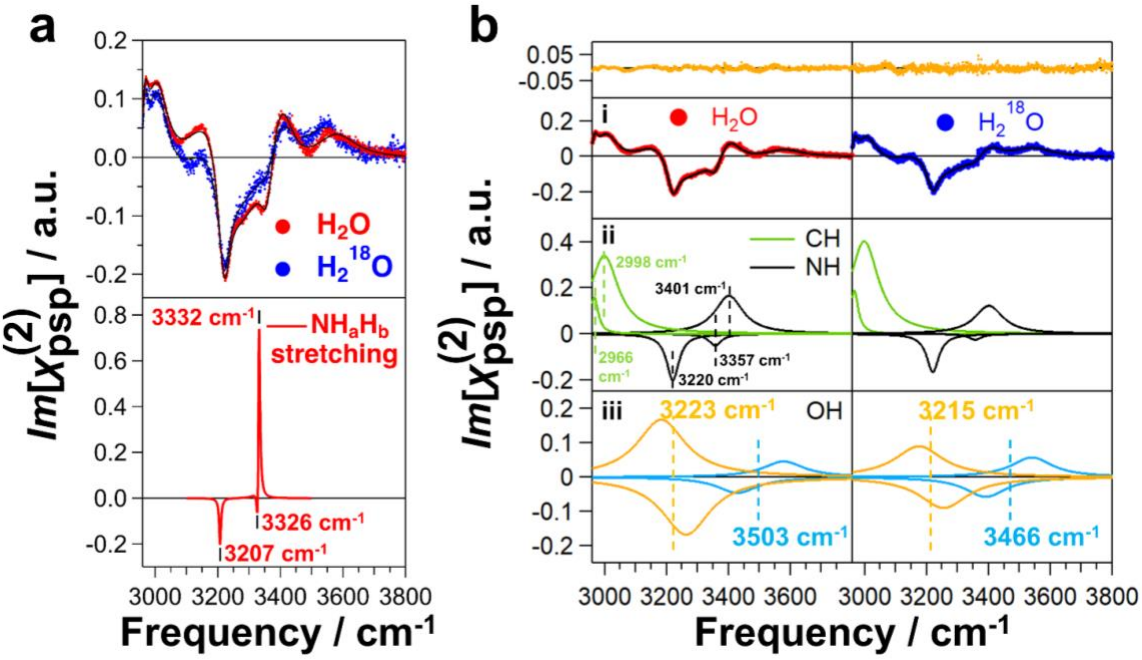

Figure 2. Experimental and calculated chiral SFG spectra of $(dA)_{12} \cdot (dT)_{12}$ dsDNA. (a) (top) Experimental chiral SFG spectra of dsDNA prepared in H_2O (red) and $H_2{}^{18}O$ (blue) obtained in the N-H/O-H stretching region with the *psp* polarization. Solid black lines are the fit to equation 2 (see Methods). (bottom) Gas-phase density functional theory (DFT) calculation of chiral SFG spectrum of dsDNA shows adenine NH_aH_b symmetric (3207 cm^{-1}) and asymmetric (3326/3332 cm^{-1}) stretching (see Figure 1b for atom labels). Note that vibrational modes due to water are not included in these DFT calculations. Calculated spectral frequencies were scaled by a factor of 0.95. Chiral SFG response from various orientations of the dsDNA relative to the plane of incidence all show chiral SFG signals of N-H stretching (see Methods and Supporting Information); the selected spectrum shown is for the Euler angles θ=20°, ψ=150°, and averaged around φ. (b) Fitting of the experimental spectra using equation 2. (b-i) Global fits (black) and residuals (yellow) of experimental chiral SFG spectra of dsDNA in H_2O (red) and $H_2{}^{18}O$ (blue). (b-ii) Fits for C-H and N-H vibrational resonances of dsDNA. (b-iii) Fits for pairs of O-H vibrational resonances of water. The averaged symmetric and asymmetric stretching frequencies are shown, which indicate red-shifts due to the isotopic $H_2{}^{18}O$ substitution, suggesting contributions of water O-H stretching modes to the chiral SFG spectra. a.u.: arbitrary units.

Experimental chiral SFG spectra of dsDNA prepared in H_2O or $H_2{}^{18}O$ are shown in Figure 2a (top panel). Global fitting of the experimental data (Figure 2b and Table S1) suggests that fitting the experimental spectra requires a minimum of five vibrational resonances of the C-H and N-H stretching of the dsDNA (Figure 2bii) and two pairs of hydration water stretching[33] (Figure 2biii). The residual analyses are shown in yellow in Figure 2b (top). Based on the vibrational frequencies, 2966 cm^{-1} and 2998 cm^{-1}, two vibrational resonances are assigned to C-H stretching modes of dsDNA (Figure 2bii, green curves). Three vibrational bands in the experimental chiral SFG spectra at 3220 cm^{-1}, 3357 cm^{-1}, and 3401 cm^{-1} (Figure 2bii, black curves) have not previously been assigned. To assign these vibrational bands, we performed gas-phase calculations of an ideal $(dA)_{12} \cdot (dT)_{12}$ dsDNA using an exciton model (see Methods and Supporting Information). The calculations (Figure 2a, bottom panel) predict the vibrational resonance at 3207 cm^{-1} is the symmetric stretching of adenine NH_aH_b, while the negative feature at 3326 cm^{-1} and the positive feature at 3332 cm^{-1} are attributed to different linear combinations of asymmetric stretching of adenine NH_aH_b groups along the dsDNA. Therefore, we propose the vibrational band at 3220 cm^{-1} in the experimental chiral SFG spectrum is symmetric stretching of adenine NH_aH_b, while the vibrational bands at 3357 cm^{-1} and 3401 cm^{-1} are asymmetric stretching modes of adenine NH_aH_b (Figure 2bii, black curves).[36]

Applying our recently developed theoretical basis for interpreting heterodyne chiral SFG spectra of water,[33] the vibrational resonances of water O-H stretching modes were modeled as pairs of vibrational resonances centered at 3223 cm^{-1} and 3503 cm^{-1} (Figure 2biii). Each pair of vibrations contains two resonances corresponding to symmetric and asymmetric O-H stretching modes of water due to intramolecular coupling. $H_2{}^{18}O$ labeling red-shifts both pairs of vibrational resonances to 3215 cm^{-1} and 3466 cm^{-1}, confirming water contributions to the chiral SFG spectrum. Because a water molecule is achiral, detection with chiral SFG implies that the hydration structures around dsDNA are chiral.

Chiral SFG is sensitive to water in the dsDNA first hydration shell.

We model the chiral SFG response of water molecules around dsDNA using a dipole-polarizability time correlation function approach with electric field mappings (Figure 3, see also Methods).[37-41] We built a molecular model of $(dA)_{12} \cdot (dT)_{12}$ dsDNA using molecular dynamics (MD) in a 52 Å × 52 Å × 73 Å box containing approximately 6400 water molecules and calculated the chiral SFG response of O-H stretching for all water molecules (Figure 3b, black curve). This calculated chiral SFG response of water spans the spectral region of ~3100-3750 cm^{-1} and supports our experimental observation of a redshift upon $H_2{}^{18}O$ substitution of vibrational features in this region (Figure 2b, panel iii). We also used the algorithm of Voronoi tessellation[32, 42, 43] (see Methods and Supporting Information) to identify water molecules in the first and second hydration shells around dsDNA. Only water molecules in the first hydration shell around dsDNA produce a chiral SFG response (Figure 3b, red curve). Remarkably, water molecules in the second hydration shell around dsDNA produce no chiral SFG response (Figure 3b, blue curve). Thus, both experiment and computation confirm that chiral SFG is sensitive to the O-H stretching modes of water molecules within the first hydration shell around dsDNA and the N-H stretching modes of adenine in $(dA)_{12} \cdot (dT)_{12}$ dsDNA.

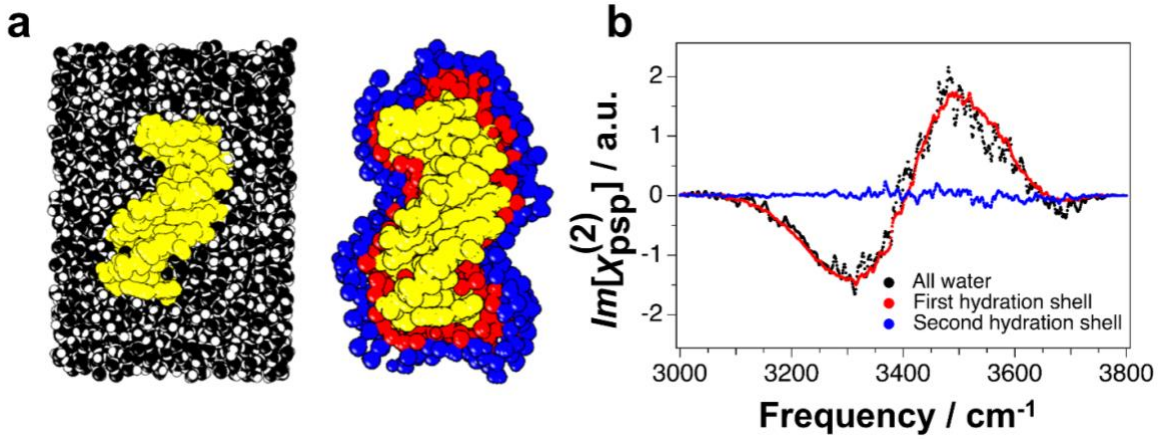

Figure 3. Chiral SFG response from water molecules surrounding $(dA)_{12} \cdot (dT)_{12}$ dsDNA in MD simulations. (a) Representative views of the MD simulations including all water molecules (black), and water molecules in the first hydration shell (red) and the second hydration shell (blue) of $(dA)_{12} \cdot (dT)_{12}$ dsDNA (yellow). The first hydration shell (red) shows signals comparable to the total chiral SFG signals (black). The second hydration shell (blue) shows almost no calculated O-H stretching response (right). Vibrational modes due to dsDNA are not included in these calculations. a.u.: arbitrary units.

Chiral SFG detects chirality transfer from dsDNA to water.

Heterodyne chiral SFG is sensitive to the macroscopic chirality of the dsDNA double helix.[28] It effectively distinguishes between native (D-) and non-native (L-) dsDNA. The chiral SFG spectra of these two enantiomers appear as mirror images of each other with opposite phase (Figure 4a). Consequently, not only do dsDNA vibrational resonances change phase, but the features assigned above to the O-H stretching of water molecules also reverse phase (Figure 4a). The chiral SFG response of water in the first hydration shell around (D-) or (L-) dsDNA is also calculated to have opposite phase (Figure 4b). Because the phase from the O-H stretching of water molecules flips with the chirality of the dsDNA, these results imply that the first hydration shell structures around (D-) and (L-) dsDNA possess opposite chirality. Thus, we have identified the origin of the chiral SFG signal of water, namely, chiral hydration structures templated by dsDNA. Furthermore, our experimental and computational results (Figure 4) establish that chiral SFG detects chirality transfer from dsDNA to the first hydration shell.

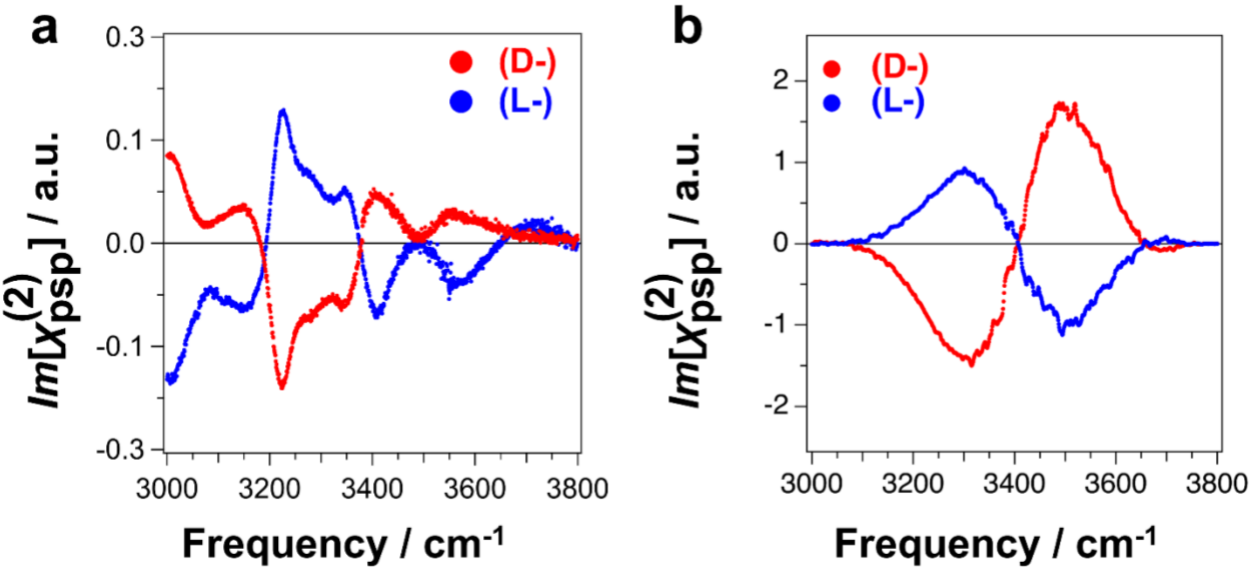

Figure 4. Native (D-) $(dA)_{12} \cdot (dT)_{12}$ dsDNA versus non-native (L-) $(dA)_{12} \cdot (dT)_{12}$ dsDNA and their hydration give mirror-image spectra confirming chirality transfer from dsDNA to hydration water. (a) Experimental chiral SFG spectra of (D-) versus (L-) dsDNA obtained in the C-H/N-H/O-H stretching region with the *psp* polarization. (b) The O-H stretching response of water molecules in the first hydration shell calculated from an MD simulation of (D-) and (L-) dsDNA. Vibrational modes due to dsDNA are not included in these calculations. a.u.: arbitrary units.

dsDNA chirality transfer to water does not propagate beyond the first hydration shell.

What is the origin of chiral SFG selectivity to the dsDNA first hydration shell? Water dipole orientation analysis[32] utilizing a 1 Å-resolution grid reveals that dsDNA creates complex chiral asymmetries in the water population in the first hydration shell (Figure 5). Furthermore, water molecules in the dsDNA second hydration shell and approximately 10-15 Å beyond the first hydration layer are ordered, but exhibit achiral $C_{\infty V}$ symmetry, which is symmetry-forbidden from generating chiral SFG response.[25, 29-31] Our analysis supports the model that chirality transfer from dsDNA to water does not propagate beyond the first hydration shell, whereas water molecules beyond the dsDNA first hydration shell are ordered by the electric field of the negatively-charged phosphate backbone. This model explains our observations (Figures 3-4) that chiral SFG is exclusively sensitive to water molecules in the first hydration shell of dsDNA.

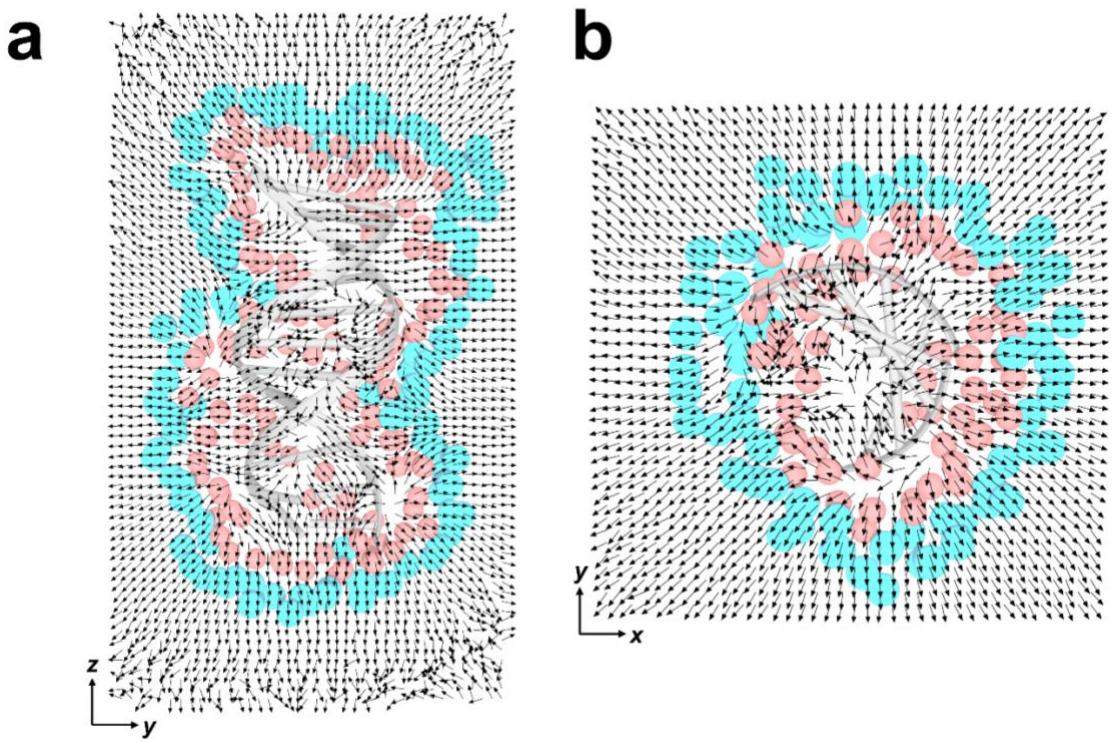

Figure 5. Mean water dipole orientations around $(dA)_{12} \cdot (dT)_{12}$ dsDNA plotted every 1 Å, averaged over 1 million frames of MD simulation. Arrows point toward the water oxygen and bisect the H-O-H angle. Representative structures for the dsDNA and the first (red) and second (blue) hydration shells are guides to the eye. The system was translated to place the DNA's centroid at the origin and rotated as described in Methods. (a) Normalized water dipoles projected onto the *yz*-plane for water molecules observed with 0.5 Å $\geq x \geq$ -0.5 Å. Note that the z = 0 Å axis crosses the 6th basepair counting from the top of the DNA structure. (b) Normalized water dipoles projected onto the *xy*-plane for water molecules observed with 0.5 Å $\geq z \geq$ -0.5 Å. The section of dsDNA structure shown corresponds to 10 Å $\geq z \geq$ -10 Å.

Chiral SFG can sense chiral hydration structures around dsDNA beyond the "spine of hydration".

To understand which subpopulations of water molecules within the first hydration shell of dsDNA contribute to the chiral SFG response, we calculated the chiral SFG spectra of different subpopulations (Figure 6a-d). We define these subpopulations using Voronoi analysis (see Methods).[42] Figure 6 shows the chiral SFG spectra of the first hydration shell, including water molecules in the minor and major grooves, and water molecules hydrating the dsDNA backbone. The average number of water molecules in each subpopulation is indicated beside the molecular models.

The total chiral SFG response of the first hydration shell (Figure 6a) is the sum of the spectral contributions of the subpopulations of water molecules hydrating the minor groove, major groove, and backbone (Figures 6b-d). Comparison of the absolute intensities of the spectra in Figures 6a and 6b shows that the O-H stretching response of water molecules in the dsDNA minor groove account for almost the entire chiral SFG response of the first hydration shell. This observation agrees with the proposed molecular origin of water signals surrounding dsDNA.[6] However, to our surprise, the simulated chiral SFG responses of water molecules hydrating the major groove (Figure 6c) and the backbone (Figure 6d) are non-zero but have nearly equal intensity and opposite phase. Thus, the sum of the spectral responses of water hydrating the major groove and backbone is nearly zero due to cancellation (Figure S2). This result reveals that not only water molecules hydrating the minor groove (Figure 6b), but also those hydrating the major groove and dsDNA backbone (Figures 6c and 6d) can contribute to the chiral SFG response (Figure 6a). This finding implies that chiral SFG can also be used to probe hydration structures of the major groove and backbone of dsDNA. Our result enhances the current understanding of the molecular origins of chiral SFG signals of water molecules hydrating dsDNA molecules. It also implies that chiral SFG can potentially distinguish different modes of small-molecule binding to dsDNA by detecting displacement of water molecules hydrating the major groove, minor groove, or backbone.

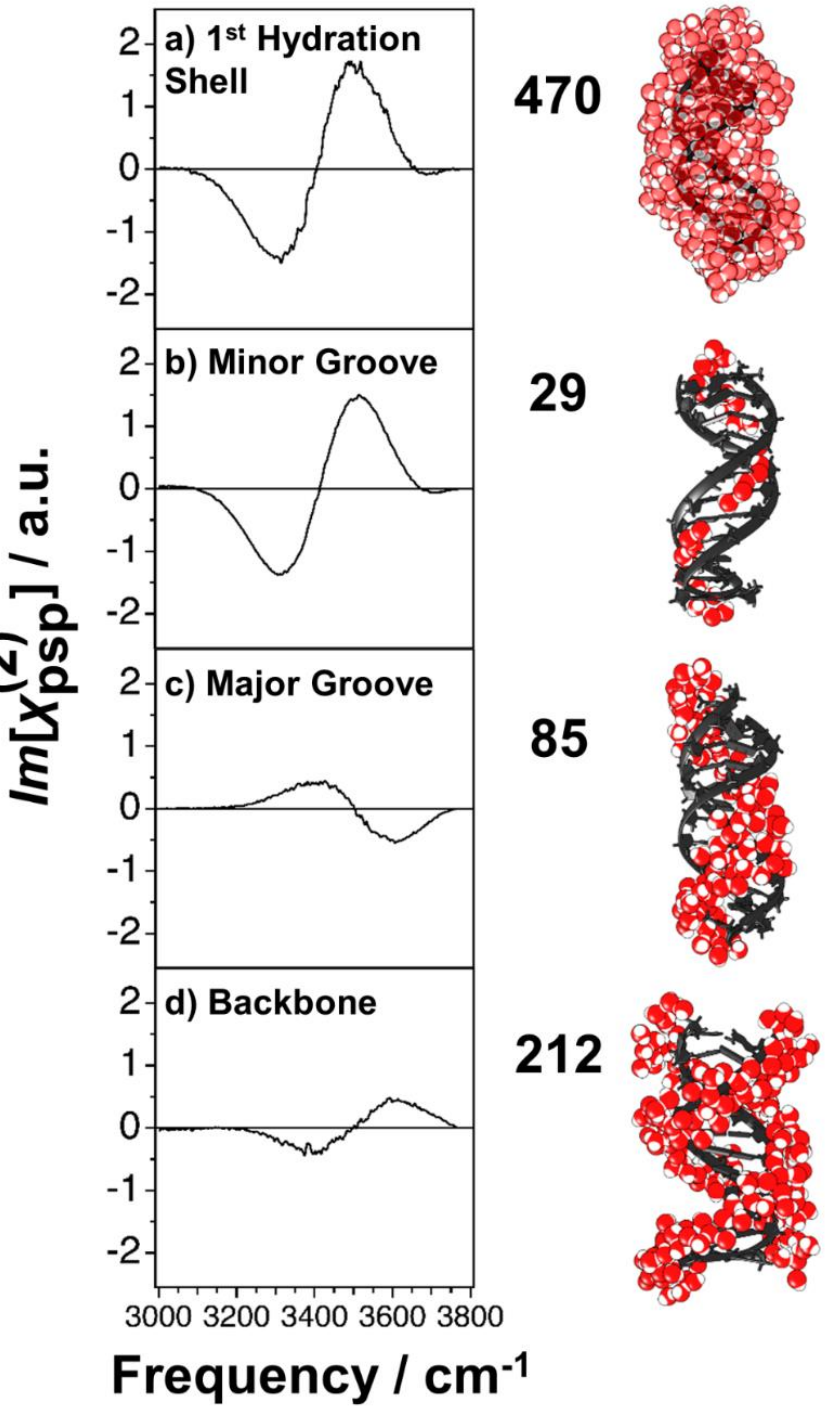

Figure 6. Calculation of the phase-sensitive chiral SFG response of the O-H stretching modes of water around $(dA)_{12} \cdot (dT)_{12}$ dsDNA corresponding to water molecules (a) in the first hydration shell, (b) along the minor groove, (c) the major groove, and (d) the backbone of dsDNA. All spectra are averaged over 1,000,000 frames from 100 ns of MD simulation. Spectral intensities can be directly compared. Note that vibrational modes due to dsDNA are not included in these calculations. The average number of water molecules per MD frame in each subset is listed. Voronoi selection[42] (see Methods) was used to identify water molecule populations around each region of the dsDNA. a.u.: arbitrary units.

Discussion

Petersen and co-workers reported the chiral SFG response of $(dAdT)_{12} \cdot (dAdT)_{12}$ dsDNA in the region 2600 – 3700 cm^{-1} and attributed the observed chiral SFG signal to water molecules embedded in the minor groove of dsDNA.[6] However, our $H_2{}^{18}O$ substitution experiment (Figure 2) and computational investigations (Figures 2-5) indicate that chiral SFG can detect the O-H stretching of chiral water assemblies around $(dA)_{12} \cdot (dT)_{12}$ dsDNA, as well as the symmetric stretching (3220 cm^{-1}) and asymmetric stretching (3357 cm^{-1} and 3401 cm^{-1}) modes of adenine NH_aH_b (Figure 2). We also detected chiral SFG response of C-H stretching modes of dsDNA (Figure 2bii). These various modes provide information about the local chemical environments and molecular structures of the dsDNA molecule.[28] Our gas-phase calculations of the chiral SFG response of $(dAdT)_{12} \cdot (dAdT)_{12}$ dsDNA (Figure S3) suggest that NH_aH_b stretching resonances are likely to have been convoluted with the O-H stretching of chiral water structures in the previously reported spectra.[6]

Our experimental and computational results reveal that dsDNA transfers chirality to the first hydration shell only (Figures 3-5). However, a loosely bound hydration shell may extend as far as 18 Å from the dsDNA surface due to the electric field of the negatively-charged phosphate backbone.[11] Our water dipole orientation analysis suggests that, beyond the first hydration shell, the electric field of the dsDNA phosphate backbone orders water in achiral $C_{\infty V}$ symmetry, which cannot generate chiral SFG response according to Simpson's chiral SFG theory (Figure 5).[20-22, 25, 29-33] Our analyses support the conclusion that chiral SFG does not report on water molecules beyond the first hydration layer of dsDNA. Therefore, we have established that chiral SFG offers a highly specific method to probe the structure of the dsDNA first hydration shell.

Dissecting the water signals from the first hydration shell around the $(dA)_{12} \cdot (dT)_{12}$ dsDNA reveals that not only minor groove water molecules, but also water subpopulations hydrating the major groove and dsDNA backbone can contribute to the experimental chiral SFG response (Figures 6a-d). However, the opposite phases and nearly equal intensities of the chiral SFG responses predicted for major groove and

backbone waters (Figures 6c and 6d) suggest that these signals can destructively interfere and cancel (Figure S2). Nonetheless, our computational findings revise the notion that the experimental chiral SFG response is only due to water molecules in the dsDNA minor groove.[6, 18] For nucleic acid duplexes with different secondary structures (for example, A-DNA or A-RNA, Z-DNA or Z-RNA, or parallel double helixes), the major groove and backbone water subpopulations might even dominate the chiral SFG response over minor groove water molecules. Alternatively, binding of proteins or other molecules to dsDNA may perturb chiral hydration structures. In such cases, the chiral SFG response of water hydrating the major groove and backbone can potentially report on molecular binding. Our work will guide further development of chiral SFG for studying molecular interactions of dsDNA.

Dickerson and co-workers originally observed the chiral "spine of hydration" in the dsDNA minor groove over 40 years ago.[2, 3] As discussed above, however, the chiral SFG response implies the existence of other chiral first hydration shell structures. The spine of hydration can now be interpreted as just one stable chiral hydration structure around dsDNA, alongside the chiral structures formed by major groove and backbone water molecules. Our findings offer an updated scientific perspective in line with recent computational work that has focused on holistic understanding of hydration structures and dynamics around dsDNA.[7, 44]

Based on our findings, chiral SFG experiments and computational analyses are now poised to address fundamental questions related to changes in dsDNA hydration structure during reactions, interactions, recognition, and binding with proteins and small molecules. Heterodyne chiral SFG reveals the phase of the water signals as well as dsDNA vibrational modes and can thereby resolve specific functional groups involved in molecular interactions with dsDNA. Our work has built a rigorous theoretical basis for interpreting chiral SFG spectra of dsDNA hydration, introducing new possibilities to use chiral hydration structures as a novel, label-free reporter for molecular binding to dsDNA.

Methods

DNA Oligomer Preparation

Cartridge-purified single-stranded DNA oligomers with sequences $(dA)_{12}$ and $(dT)_{12}$ were purchased from the Keck Oligonucleotide Synthesis Resource at Yale University and used without further purification. For all experiments, solutions of double-stranded DNA oligomers were prepared at 100 μM, heated in a water bath at 80 ºC for 10 minutes, and allowed to cool in the water bath overnight. Solutions were subsequently stored at 4 ºC.

Vibrational SFG Measurements

Solutions of dsDNA oligomers were prepared in H_2O or $H_2{}^{18}O$ (Sigma-Aldrich, 97 atom % ^{18}O). For all SFG experiments, 10 μL was applied to the clean surface of a right-handed z-cut α-quartz crystal and the solution was dried in a desiccator. To prevent exchange of $H_2{}^{18}O$ with ambient humidity in hydrated dsDNA films, samples were dried in a sealed container with desiccant under a positive pressure nitrogen flow.

Phase-resolved chiral SFG[45-49] was used to probe hydrated dsDNA films at the quartz surface with the *psp* polarization (*p*-polarized sum frequency, *s*-polarized visible, *p*-polarized infrared) using a homebuilt broadband spectrophotometer. A Ti:Sapphire regenerative amplifier (Astrella F, Coherent, CA) generates 9 W of 800 nm output with a repetition rate of 5 kHz and 100-fs pulse width. The output is split to generate the tunable IR source by pumping an optical parametric amplifier (OPA) (TOPAS-PRIME, Coherent, CA). This OPA is coupled to a non-collinear difference frequency generator (NDFG, Coherent, CA), which generates broadband infrared pulses tunable from 2.4 to 11 μm, corresponding to the range of ~900 - 4000 cm^{-1}. The remainder of the 800 nm amplifier output enters a 4f pulse shaper for a final pulse duration <10 ps. The beams are directed to be coincident on the sample surface spatially and temporally to generate SFG signal. The temporal overlap is achieved by a delay stage to change the path length of the infrared beam. The SFG signal generated from the sample surface is collected by a collimating lens and focused into a

spectrograph before being detected by a cryogenically cooled CCD camera. The infrared source is *p*-polarized upon exiting the NDFG, while the visible and SFG polarizations are selected using a waveplate and a polarizer.

Chiral SFG spectra were collected with the quartz oriented along the +*y* and -*y* axes of the quartz as calibrated in the laboratory frame (see SI).[20] Unless noted otherwise, 4 spectra (5 minutes each) were acquired along both the +*y* and -*y* axes and normalized by the clean quartz surface. To obtain the purely imaginary component ($Im[\chi^{(2)}]$) of the vibrational SFG response, the averages of the normalized measurements along the +*y* and -*y* axes were subtracted according to:

$$Im[\chi^{(2)}] = \frac{(I_{+y} - I_{-y})}{4} \tag{1}$$

The frequency of SFG spectra were calibrated using polystyrene (Buck Scientific; 0.05 mm film). Spikes of signals due to cosmic rays were manually removed.

The spectra were analyzed using equation 2 to model the vibrational resonances. The first term in this expression fits the spectral contributions from C-H and N-H stretches of the dsDNA, where ω_{IR} is the frequency of the incident infrared beam, and ω_q, Γ_q, and A_q are the frequency of the vibrational resonance, the damping factor, and the amplitude of the q^{th} vibrational mode, respectively.

$$Im[\chi^{(2)}] \propto \left[\sum_q \frac{A_q}{(\omega_{IR} - \omega_q - i\Gamma_q)} + \sum_n \frac{A_n}{\left(\omega_{IR} - \left(\omega_n - \frac{1}{2}\Delta\nu\right) - i\Gamma_n\right)} - \frac{A_n}{\left(\omega_{IR} - \left(\omega_n + \frac{1}{2}\Delta\nu\right) - i\Gamma_n\right)}\right] \tag{2}$$

The second term in equation 2 is used to fit the O-H stretching modes. In our previous report,[33] we demonstrated that the chiral SFG responses from water result from intramolecular coupling, causing the symmetric and asymmetric stretching modes of water to appear as two non-degenerate Lorentzian peaks with opposite phase, equal magnitude, and displaced frequency. This term fits the n^{th} pair of the symmetric

and asymmetric O-H stretching modes of water using shared parameters for amplitude (A_n) and width (Γ_n). The peak positions for both symmetric and asymmetric stretching modes are defined using two parameters, the resonant frequency (ω_n) and the frequency difference ($\Delta\nu$) between the symmetric and asymmetric stretching modes.

Equation 2 was used to globally fit spectra of dsDNA in H_2O and $H_2{}^{18}O$, where the peak positions and widths for all N-H and C-H stretching modes were linked, and the width and frequency differences for all pairs of O-H stretching modes were linked. The value of $\Delta\nu$ was constrained to be between 30 cm^{-1} and 150 cm^{-1} based on previous studies.[33]

The fitting model used in this work is guided by our previous report,[33] which found that the chiral SFG response of a water OH stretching band can be described by an "up-down" or "down-up" (doublet) lineshape due to the C_{2v} symmetry of a water molecule. A similar lineshape was observed for coupled C=O oscillators in dsDNA when using vibrational circular dichroism by the Zanni group.[50] Despite local C_{2v} symmetry of the NH_aH_b group on adenine (see Figure 1 for atom labeling), the N-H symmetric and asymmetric stretches need not be fit with the doublet model. Greve *et al.*[51] showed significant vibrational coupling between the N3-H_c and NH_2 modes that removes the local mode symmetry. They found adding this coupling and Fermi resonance with the C6-NH_2 bending mode to be necessary to replicate experimental spectra. Furthermore, any coupling from stacking base pairs would further remove the C_{2v} local symmetry. Lastly, the NH_2 is bonded to an aromatic system in the nucleobase. The doublet fitting model for chiral SFG response of water was derived[33] based on the individual bond polarizabilities having only diagonal terms (α_{aa}, α_{bb}, and α_{cc}) and the resulting molecular hyperpolarizability containing only the effects of the rotated C_∞ bonds. An aromatic system conjugated with the chromophore will likely contribute to the Raman tensor of the system within the plane of conjugation; this means that the system's β (hyperpolarizability) cannot be well represented as the sum of individual bonds, disrupting the model that would produce a doublet.

Density Functional Theory Calculations

Density functional theory (DFT) calculations were performed on AT Watson-Crick base pairs using the ωB97XD functional[52] and the cc-pvdz basis set[53] using Gaussian 16, Rev. C01.[54] A partial solvated model including an explicit water molecule was used to account for the solvation of the NH_2 group on the adenine[55, 56] (see Figure S4). Harmonic analyses were performed to compute normal modes, frequencies, transition dipole moments, and transition Raman polarizability tensors for spectroscopic characterization. See Supporting Information for additional details.

Exciton Model

To account for coupling between different AT base pairs in the SFG spectra, we model the $(dA)_{12} \cdot (dT)_{12}$ dsDNA using a coupled exciton Hamiltonian of the form[57, 58]

$$H = \sum_{j=1}^{n} \sum_{m_j} \hbar\omega_{m_j} a_{m_j}^{+} a_{m_j} + \sum_{j=1}^{n} \sum_{k>j}^{n} \sum_{m_j} \sum_{m_k} \hbar J_{m_j m_k} a_{m_j}^{+} a_{m_k} + c.c. \quad (3)$$

where n is the total number of base pairs, ω_{m_j} represents the m_j-th local mode frequency in the j-th base pair, $J_{m_j m_k}$ represents the inter-strand vibrational coupling between the m_j-th and m_k-th vibrational modes in the j-th and k-th base pair, and $a_{m_j}^{+}$ and a_{m_j} are creation and annihilation operators of the m_j-th mode. In our model, local mode bases are chosen as the normal modes of a single AT Watson-Crick base pair. Local mode frequencies and coupling parameters were determined using the Hessian matrix reconstruction method,[59-61] where only interactions between first- and second-neighbor base pairs were considered. Simulation and parameterization details are provided in the Supporting Information.

Calculations of dsDNA NH Chiral SFG Spectrum

Our approach for simulating SFG spectra has been previously described.[62-65] Here, we provide only a brief summary. The calculation involves the determination of the second-order molecular

hyperpolarizabilities $\beta^{(2)}_{ijk,q} = \alpha_{ij,q}\mu_{k,q}$, where $\alpha_{ij,q}$ and $\mu_{k,q}$ (with $i,j,k = x,y,z$) are elements of the transition polarizability and dipole moment of the q-th exciton in the molecular frame, respectively. The hyperpolarizability $\beta^{(2)}_{ijk,q}$ is then rotated to the laboratory frame ($I,J,K = X,Y,Z$) and averaged over the azimuthal angle ϕ in 5° increments to obtain the second-order susceptibility $\chi^{(2)}_{IJK,q} = \sum_{ijk}\langle R_{Ii}R_{Jj}R_{Kk}\rangle\beta^{(2)}_{ijk,q}$, where R_{Ii} represent elements of the ZYZ Euler rotation matrix.[25] The heterodyne SFG spectrum is computed as

$$Im[\chi^{(2)}](\omega_{IR}) = \mathrm{Im}\sum_{q}\frac{\chi^{(2)}_{psp,q}}{\omega_{IR} - \omega_q + i\Gamma_q} \tag{4}$$

where ω_q is the frequency of the q-th exciton vibrational mode and the effective *psp* susceptibilities are given by[25]

$$\chi^{(2)}_{psp,q} = L_{ZYX}\chi^{(2)}_{ZYX,q} - L_{XYZ}\chi^{(2)}_{XYZ,q} \tag{5}$$

where L_{ijk} are Fresnel factors that depend on the refractive index of the interface as well as the incident angle of the lasers.[66, 67] The Fresnel factors used in this study are listed in **Table S3**. The harmonic frequencies were scaled by 0.95, and Γ_q was set to 4.0 cm^{-1} to facilitate comparisons with experiments.

Molecular Dynamics Simulations

The AMBER tool[68] Nucleic Acid Builder was used to build a $(dA)_{12} \cdot (dT)_{12}$ B-DNA molecule. The AMBER tool *tleap* was used to solvate and neutralize the system with TIP4P-Ew water[69] and sodium ions, leaving at least 15 Å of solvent on all sides of the dsDNA. The system was then minimized with restraints on the dsDNA (force constant 200 kcal/mol/Å^2). This was followed by 500 ps of solvent equilibration with restraints on the dsDNA (200 kcal/mol/Å^2). Then the system was minimized with restraints on the heavy atoms in the dsDNA (100 kcal/mol/Å^2). Following this, the system was minimized in three phases with

restraints on the dsDNA backbone gradually being released (100 kcal/mol/Å^2, then 50 kcal/mol/Å^2, then 10 kcal/mol/Å^2). This was followed by a minimization of the entire system without restraints. This minimization was followed by 360 ps of temperature annealing in the NPT ensemble (1.01325 bar, 1 atm) to heat the system from 0 K to 300 K. Then the system was equilibrated in the NPT ensemble for 5 ns, and finally the system was equilibrated for 5 ns in the NVT ensemble. All energy minimizations used a combination of steepest descent and conjugate gradient approaches. For production runs, the system was propagated for 100 ns in the NVT ensemble, saving conformations every 100 fs. All dynamics used a Langevin integrator with a friction coefficient of 1/picosecond, a temperature of 300 K, and a timestep of 1 fs. The OL15 force field[70] was used for the dsDNA. The particle-mesh Ewald method[71] was used to calculate long-range electrostatic interactions. Other nonbonded interactions were cut off at 14 Å. Hydrogen-containing bonds within the dsDNA were constrained with the SHAKE algorithm,[72] and the water molecules were kept rigid with the SETTLE method.[73] All minimizations were performed using AMBER pmemd.MPI on 4 CPUs, and all dynamics runs were performed on Nvidia GPUs using CUDA 10.1 and AMBER pmemd.cuda.[68]

Calculations of Water Chiral SFG Spectrum

SFG spectra were calculated as described previously using Skinner's electric field mapping method[38, 40, 41] and the inhomogeneous (non-time-dependent) limit approximation to the time-correlation function. Only water molecules in a selected subset (see below) were represented in the exciton Hamiltonian, but all atoms in the system contributed to the electric field experienced by each O-H group in the selected subset. Prior to the calculation of dipoles and polarizabilities, the system was rotated so that the sixth thymine's N3-H3 bond pointed along the *y*-axis with the hydrogen atom facing in the positive direction. The *x*-axis faced in the same general direction as O2; any component in the *y*- direction was removed to make the vector perpendicular to the *y*-axis. The *z*-axis then faced approximately along the dsDNA helix axis. The entire $\chi^{(2)}$ tensor was calculated to allow for transformation to another coordinate system. The tensor was rotated using the Euler angles ϕ, θ, and ψ with the *zyz* convention. The tensor was

averaged over all values of ϕ using 100 subconformations while being rotated to θ = 20° to match the conformation used in the *ab initio* calculations. The ψ angle had a minimal effect on the spectra and was thus set to 0. The *psp* response was calculated as $\chi^{(2)}_{zyx} - \chi^{(2)}_{xyz}$. The vanishing of the quantity $\chi^{(2)}_{zyz} - \chi^{(2)}_{xyx}$ was monitored to ensure C_∞ symmetry was approximately achieved by integration over ϕ.[30] Note that, because the orientation of dsDNA relative to the interface in our experiments is unknown, the absolute phases of the calculated water spectra are ambiguous with respect to experiment. However, the relative phases and amplitudes of the calculated water spectra are directly comparable to experiment. Accordingly, all calculated spectra of water around $(dA)_{12} \cdot (dT)_{12}$ dsDNA were multiplied by a factor of -1 to capture the absolute phases observed in experiments.

Analysis of Water Dipole Orientation

The water dipole orientation analysis was performed using the MD simulation prepared as described in previous sections. The simulation box was divided into a 40 Å × 40 Å × 70 Å grid centered on the origin with 1 Å spacing. For each frame, the entire system was translated to move the dsDNA's centroid to the origin and then rotated. Each water was assigned to the grid cell in which its oxygen was located. The dipole moment vector of all waters within each cell was summed over the frames and then divided by the number of waters to yield a mean molecular dipole vector. The mean molecular dipole vector was calculated from partial positive charge to partial negative charge on each water molecule, and therefore the arrows point radially outward from the negatively-charged dsDNA. For visualization, representative structures for the first and second hydration shells were selected via Voronoi tessellation (see next section),[42] and the dsDNA geometry was averaged over all frames. Water molecules are depicted as the van der Waals spheres of their oxygen atoms. UCSF Chimera[74] was used to generate the corresponding figures. In Figure 5a, a slice of the hydration shells with -5 Å ≤ x ≤ 0 Å was taken and is shown as spheres; mean dipole vectors in grid cells centered on x = 0 Å were projected onto the yz-plane and normalized. In Figure

5b, a slice of the hydration shells with -5 Å ≤ z ≤ 0 Å was taken and is shown as spheres; mean dipole vectors in grid cells centered on z = 0 Å were projected onto the *xy*-plane and normalized.

Selection of Water Molecule Subsets

Water molecules in the first hydration shell were identified using Voronoi tessellation.[42] Voronoi tessellation defines cells for each atom consisting of the points closer to that atom than to any other atom; this allows for the identification of "neighbors" to any group of atoms. Within the set of first hydration shell water molecules, water subpopulations belonging to the dsDNA minor groove, major groove, and backbone were identified as follows:

(a) **Major groove water molecules** were defined as water molecules closer to an atom of the major groove than to any other atom group in dsDNA.

(b) **Minor groove water molecules** were defined as water molecules within 3.5 Å of the H2 atom on adenine.

(c) **Backbone water molecules** were selected in two steps. First, based on distance, all water molecules closer to backbone atoms than to major- or minor-groove atoms were selected. This produced a selection of water molecules (*selection backbone*$_1$) along the backbone, as well as some water molecules near, but not inside, the minor groove. In the second step, these water molecules near the minor groove were removed using Voronoi tessellation.[42] From *selection backbone*$_1$ Voronoi tessellation was used to identify water molecules that neighbored the subset of minor groove water molecules (defined previously in b), as well as water molecules neighboring the neighbors of minor groove water molecules. All these water molecules were removed from *selection backbone*$_1$. The remaining water molecules are defined as backbone water molecules. This two-step selection process was to avoid contamination from water molecules inside or proximal to the minor groove.

All atom selections were made using the MDAnalysis library[75] and in-house Python code. The freud library[76] was used to access the Voronoi tessellation code voro++ from Python.[77]

Supporting Information

The following materials are included in the Supporting Information (PDF):

Raw experimental chiral SFG spectra of $(dA)_{12} \cdot (dT)_{12}$ dsDNA prepared in H_2O and in $H_2{}^{18}O$; fitting parameters for chiral SFG spectra of $(dA)_{12} \cdot (dT)_{12}$ dsDNA prepared in H_2O and in $H_2{}^{18}O$; summation of the calculated chiral SFG spectra of water molecules hydrating the backbone and major groove of $(dA)_{12} \cdot (dT)_{12}$ dsDNA; calculated chiral SFG spectrum of the N-H stretching response of $(dAdT)_{12} \cdot (dTdA)_{12}$ dsDNA; complete description of density functional theory and exciton model calculations and parameters; orientational dependencies of the calculated chiral SFG spectra of the N-H stretching response of $(dA)_{12} \cdot (dT)_{12}$ dsDNA.

Acknowledgments

The authors acknowledge Garth Simpson (Purdue University) and Martin Zanni (University of Wisconsin-Madison) for insightful comments during the preparation of this manuscript. E.A.P. was supported by the NIH (5T32GM008283-31) and a John C. Tully Chemistry Research Fellowship. D.K. was supported by the NIH (5T32GM008283-32). L.V. acknowledges support from NSF (CHE-1753207). V.S.B. acknowledges support from the NSF-CCI Center for Quantum Dynamics on Modular Quantum Devices (CQD-MQD) (CHE-2124511). S.H.-S. acknowledges support by the National Institutes of Health Grant No. R35 GM139449. E.C.Y.Y. acknowledges NSF support (CHE-1905169).

References

(1) Watson, J. D.; Crick, F. H. "Molecular structure of nucleic acids: a structure for deoxyribose nucleic acid," *Nature* 171(4356), 737-738 (1953). https://doi.org/10.1038/171737a0

(2) Dickerson, R.; Drew, H.; Conner, B. *Biomolecular Stereodynamics*; Adenine Press, 1981.

(3) Kopka, M. L.; Fratini, A. V.; Drew, H. R.; Dickerson, R. E. "Ordered water structure around a B-DNA dodecamer: A quantitative study," *Journal of Molecular Biology* 163(1), 129-146 (1983). https://doi.org/10.1016/0022-2836(83)90033-5

(4) Chuprina, V. P. "Anomalous structure and properties of poly (dA)·poly(dT). Computer simulation of the polynucleotide structure with the spine of hydration in the minor groove," *Nucleic Acids Research* 15(1), 293-311 (1987). https://doi.org/10.1093/nar/15.1.293

(5) Liepinsh, E.; Otting, G.; Wüthrich, K. "NMR observation of individual molecules of hydration water bound to DNA duplexes: direct evidence for a spine of hydration water present in aqueous solution," *Nucleic Acids Research* 20(24), 6549-6553 (1992). https://doi.org/10.1093/nar/20.24.6549

(6) McDermott, M. L.; Vanselous, H.; Corcelli, S. A.; Petersen, P. B. "DNA's Chiral Spine of Hydration," *ACS Central Science* 3(7), 708-714 (2017). https://doi.org/10.1021/acscentsci.7b00100

(7) Duboué-Dijon, E.; Fogarty, A. C.; Hynes, J. T.; Laage, D. "Dynamical Disorder in the DNA Hydration Shell," *Journal of the American Chemical Society* 138(24), 7610-7620 (2016). https://doi.org/10.1021/jacs.6b02715

(8) Tao, N. J.; Lindsay, S. M.; Rupprecht, A. "Structure of DNA hydration shells studied by Raman spectroscopy," *Biopolymers* 28(5), 1019-1030 (1989). https://doi.org/10.1002/bip.360280509

(9) Perera, P.; Wyche, M.; Loethen, Y.; Ben-Amotz, D. "Solute-Induced Perturbations of Solvent-Shell Molecules Observed Using Multivariate Raman Curve Resolution," *Journal of the American Chemical Society* 130(14), 4576-4577 (2008). https://doi.org/10.1021/ja077333h

(10) Elsaesser, T.; Schauss, J.; Kundu, A.; Fingerhut, B. P. "Phosphate Vibrations Probe Electric Fields in Hydrated Biomolecules: Spectroscopy, Dynamics, and Interactions," *The Journal of Physical Chemistry B* 125(15), 3899-3908 (2021). https://doi.org/10.1021/acs.jpcb.1c01502

(11) Singh, A. K.; Wen, C.; Cheng, S.; Vinh, N. Q. "Long-range DNA-water interactions," *Biophysical Journal* 120(22), 4966-4979 (2021). https://doi.org/10.1016/j.bpj.2021.10.016

(12) Pal, S. K.; Zhao, L.; Zewail, A. H. "Water at DNA surfaces: Ultrafast dynamics in minor groove recognition," *Proceedings of the National Academy of Sciences* 100(14), 8113 (2003). https://doi.org/10.1073/pnas.1433066100

(13) Yang, M.; Szyc, Ł.; Elsaesser, T. "Decelerated Water Dynamics and Vibrational Couplings of Hydrated DNA Mapped by Two-Dimensional Infrared Spectroscopy," *The Journal of Physical Chemistry B* 115(44), 13093-13100 (2011). https://doi.org/10.1021/jp208166w

(14) Laage, D.; Elsaesser, T.; Hynes, J. T. "Water Dynamics in the Hydration Shells of Biomolecules," *Chemical Reviews* 117(16), 10694-10725 (2017). https://doi.org/10.1021/acs.chemrev.6b00765

(15) Wurpel, G. W. H.; Sovago, M.; Bonn, M. "Sensitive Probing of DNA Binding to a Cationic Lipid Monolayer," *Journal of the American Chemical Society* 129(27), 8420-8421 (2007). https://doi.org/10.1021/ja072552o

(16) Singh, P. C.; Ahmed, M.; Nihonyanagi, S.; Yamaguchi, S.; Tahara, T. "DNA-Induced Reorganization of Water at Model Membrane Interfaces Investigated by Heterodyne-Detected Vibrational Sum Frequency Generation Spectroscopy," *The Journal of Physical Chemistry B* 126(4), 840-846 (2022). https://doi.org/10.1021/acs.jpcb.1c08581

(17) Levinson, N. M.; Bolte, E. E.; Miller, C. S.; Corcelli, S. A.; Boxer, S. G. "Phosphate Vibrations Probe Local Electric Fields and Hydration in Biomolecules," *Journal of the American Chemical Society* 133(34), 13236-13239 (2011). https://doi.org/10.1021/ja2042589

(18) Perets, E. A.; Yan, E. C. Y. "The H2O Helix: The Chiral Water Superstructure Surrounding DNA," *ACS Central Science* 3(7), 683-685 (2017). https://doi.org/10.1021/acscentsci.7b00229

(19) Perets, E. A.; Yan, E. C. Y. "Chiral Water Superstructures around Antiparallel β-Sheets Observed by Chiral Vibrational Sum Frequency Generation Spectroscopy," *The Journal of Physical Chemistry Letters* 10(12), 3395-3401 (2019). https://doi.org/10.1021/acs.jpclett.9b00878

(20) Perets, E. A.; Konstantinovsky, D.; Fu, L.; Chen, J.; Wang, H.-F.; Hammes-Schiffer, S.; Yan, E. C. Y. "Mirror-image antiparallel β-sheets organize water molecules into superstructures of opposite chirality," *Proceedings of the National Academy of Sciences* 117(52), 32902 (2020). https://doi.org/10.1073/pnas.2015567117

(21) Konstantinovsky, D.; Perets, E. A.; Yan, E. C. Y.; Hammes-Schiffer, S. "Simulation of the Chiral Sum Frequency Generation Response of Supramolecular Structures Requires Vibrational Couplings," *The Journal of Physical Chemistry B* 125(43), 12072-12081 (2021). https://doi.org/10.1021/acs.jpcb.1c06360

(22) Yan, E. C. Y.; Perets, E. A.; Konstantinovsky, D.; Hammes-Schiffer, S. "Detecting Interplay of Chirality, Water, and Interfaces for Elucidating Biological Functions," *Accounts of Chemical Research* 56(12), 1494-1504 (2023). https://doi.org/10.1021/acs.accounts.3c00088

(23) Wang, J.; Chen, X.; Clarke, M. L.; Chen, Z. "Detection of chiral sum frequency generation vibrational spectra of proteins and peptides at interfaces in situ," *Proceedings of the National Academy of Sciences of the United States of America* 102(14), 4978 (2005). https://doi.org/10.1073/pnas.0501206102

(24) Wang, Z.; Fu, L.; Yan, E. C. Y. "C–H Stretch for Probing Kinetics of Self-Assembly into Macromolecular Chiral Structures at Interfaces by Chiral Sum Frequency Generation Spectroscopy," *Langmuir* 29(12), 4077-4083 (2013). https://doi.org/10.1021/la304954h

(25) Yan, E. C. Y.; Fu, L.; Wang, Z.; Liu, W. "Biological Macromolecules at Interfaces Probed by Chiral Vibrational Sum Frequency Generation Spectroscopy," *Chemical Reviews* 114(17), 8471-8498 (2014). https://doi.org/10.1021/cr4006044

(26) Perets, E. A.; Videla, P. E.; Yan, E. C. Y.; Batista, V. S. "Chiral Inversion of Amino Acids in Antiparallel β-Sheets at Interfaces Probed by Vibrational Sum Frequency Generation Spectroscopy," *The Journal of Physical Chemistry B* 123(27), 5769-5781 (2019). https://doi.org/10.1021/acs.jpcb.9b04029

(27) Stokes, G. Y.; Gibbs-Davis, J. M.; Boman, F. C.; Stepp, B. R.; Condie, A. G.; Nguyen, S. T.; Geiger, F. M. "Making “Sense” of DNA," *Journal of the American Chemical Society* 129(24), 7492-7493 (2007). https://doi.org/10.1021/ja071848r

(28) Perets, E. A.; Olesen, K. B.; Yan, E. C. Y. "Chiral Sum Frequency Generation Spectroscopy Detects Double-Helix DNA at Interfaces," *Langmuir* 38(18), 5765-5778 (2022). https://doi.org/10.1021/acs.langmuir.2c00365

(29) Simpson, G. J. "Molecular origins of the remarkable chiral sensitivity of second-order nonlinear optics," *ChemPhysChem* 5(9), 1301-1310 (2004). https://doi.org/10.1002/cphc.200300959

(30) Moad, A. J.; Simpson, G. J. "A unified treatment of selection rules and symmetry relations for sum-frequency and second harmonic spectroscopies," *The Journal of Physical Chemistry B* 108(11), 3548-3562 (2004). https://doi.org/10.1021/jp035362i

(31) Simpson, G. J. *Nonlinear optical polarization analysis in chemistry and biology*; Cambridge University Press, 2017.

(32) Konstantinovsky, D.; Perets, E. A.; Santiago, T.; Velarde, L.; Hammes-Schiffer, S.; Yan, E. C. Y. "Detecting the First Hydration Shell Structure around Biomolecules at Interfaces," *ACS Central Science* 8(10), 1404-1414 (2022). https://doi.org/10.1021/acscentsci.2c00702

(33) Konstantinovsky, D.; Santiago, T.; Tremblay, M.; Simpson, G. J.; Hammes-Schiffer, S.; Yan, E. C. Y. "Theoretical basis for interpreting heterodyne chirality-selective sum frequency generation spectra of water," *The Journal of Chemical Physics* 160(5), 055102 (2024). https://doi.org/10.1063/5.0181718

(34) Li, Z.; Weeraman, C. N.; Azam, M. S.; Osman, E.; Gibbs-Davis, J. M. "The thermal reorganization of DNA immobilized at the silica/buffer interface: a vibrational sum frequency generation investigation," *Physical Chemistry Chemical Physics* 17(19), 12452-12457 (2015), 10.1039/C5CP00781J. https://doi.org/10.1039/C5CP00781J

(35) Jung, S.-Y.; Lim, S.-M.; Albertorio, F.; Kim, G.; Gurau, M. C.; Yang, R. D.; Holden, M. A.; Cremer, P. S. "The Vroman effect: a molecular level description of fibrinogen displacement," *Journal of the American Chemical Society* 125(42), 12782-12786 (2003). https://doi.org/10.1021/ja037263o

(36) Yang, M.; Szyc, Ł.; Elsaesser, T. "Femtosecond Two-Dimensional Infrared Spectroscopy of Adenine-Thymine Base Pairs in DNA Oligomers," *The Journal of Physical Chemistry B* 115(5), 1262-1267 (2011). https://doi.org/10.1021/jp1090697

(37) Morita, A.; Hynes, J. T. "A Theoretical Analysis of the Sum Frequency Generation Spectrum of the Water Surface. II. Time-Dependent Approach," *The Journal of Physical Chemistry B* 106(3), 673-685 (2002). https://doi.org/10.1021/jp0133438

(38) Auer, B. M.; Skinner, J. L. "Dynamical effects in line shapes for coupled chromophores: Time-averaging approximation," *The Journal of Chemical Physics* 127(10), 104105 (2007). https://doi.org/10.1063/1.2766943

(39) Auer, B. M.; Skinner, J. L. "IR and Raman spectra of liquid water: Theory and interpretation," *The Journal of Chemical Physics* 128(22), 224511 (2008). https://doi.org/10.1063/1.2925258

(40) Auer, B. M.; Skinner, J. L. "Vibrational Sum-Frequency Spectroscopy of the Water Liquid/Vapor Interface," *The Journal of Physical Chemistry B* 113(13), 4125-4130 (2009). https://doi.org/10.1021/jp806644x

(41) Pieniazek, P. A.; Tainter, C. J.; Skinner, J. L. "Interpretation of the water surface vibrational sum-frequency spectrum," *The Journal of Chemical Physics* 135(4), 044701 (2011). https://doi.org/10.1063/1.3613623

(42) Konstantinovsky, D.; Yan, E. C. Y.; Hammes-Schiffer, S. "Characterizing Interfaces by Voronoi Tessellation," *The Journal of Physical Chemistry Letters* 14(23), 5260-5266 (2023). https://doi.org/10.1021/acs.jpclett.3c01159

(43) Rosu-Finsen, A. "Interfacial interpretation," *Nature Reviews Chemistry* 7(7), 461-461 (2023). https://doi.org/10.1038/s41570-023-00518-6

(44) Furse, K. E.; Corcelli, S. A. "Effects of an Unnatural Base Pair Replacement on the Structure and Dynamics of DNA and Neighboring Water and Ions," *The Journal of Physical Chemistry B* 114(30), 9934-9945 (2010). https://doi.org/10.1021/jp105761b

(45) Shen, Y. R. "Surface properties probed by second-harmonic and sum-frequency generation," *Nature* 337(6207), 519-525 (1989). https://doi.org/10.1038/337519a0

(46) Ji, N.; Ostroverkhov, V.; Chen, C.-Y.; Shen, Y.-R. "Phase-Sensitive Sum-Frequency Vibrational Spectroscopy and Its Application to Studies of Interfacial Alkyl Chains," *Journal of the American Chemical Society* 129(33), 10056-10057 (2007). https://doi.org/10.1021/ja071989t

(47) Shen, Y. R. "Phase-Sensitive Sum-Frequency Spectroscopy," *Annual Review of Physical Chemistry* 64(NA), 129-150 (2013). https://doi.org/10.1146/annurev-physchem-040412-110110

(48) Fu, L.; Chen, S.-L.; Wang, H.-F. "Validation of Spectra and Phase in Sub-1 cm–1 Resolution Sum-Frequency Generation Vibrational Spectroscopy through Internal Heterodyne Phase-Resolved Measurement," *The Journal of Physical Chemistry B* 120(8), 1579-1589 (2016). https://doi.org/10.1021/acs.jpcb.5b07780

(49) Chen, S.-L.; Fu, L.; Gan, W.; Wang, H.-F. "Homogeneous and inhomogeneous broadenings and the Voigt line shapes in the phase-resolved and intensity sum-frequency generation vibrational spectroscopy," *The Journal of Chemical Physics* 144(3), 034704 (2016). https://doi.org/10.1063/1.4940145

(50) Krummel, A. T.; Zanni, M. T. "Interpreting DNA Vibrational Circular Dichroism Spectra Using a Coupling Model from Two-Dimensional Infrared Spectroscopy," *The Journal of Physical Chemistry B* 110(48), 24720-24727 (2006). https://doi.org/10.1021/jp063227a

(51) Greve, C.; Preketes, N. K.; Fidder, H.; Costard, R.; Koeppe, B.; Heisler, I. A.; Mukamel, S.; Temps, F.; Nibbering, E. T. J.; Elsaesser, T. "N–H Stretching Excitations in Adenosine-Thymidine Base Pairs in Solution: Pair Geometries, Infrared Line Shapes, and Ultrafast Vibrational Dynamics," *The Journal of Physical Chemistry A* 117(3), 594-606 (2013). https://doi.org/10.1021/jp310177e

(52) Chai, J.-D.; Head-Gordon, M. "Long-range corrected hybrid density functionals with damped atom–atom dispersion corrections," *Phys. Chem. Chem. Phys.* 10(44), 6615-6620 (2008), 10.1039/B810189B. https://doi.org/10.1039/B810189B

(53) Dunning, T. H., Jr. "Gaussian basis sets for use in correlated molecular calculations. I. The atoms boron through neon and hydrogen," *J. Chem. Phys.* 90(2), 1007-1023 (1989). https://doi.org/10.1063/1.456153

(54) Gaussian 16, Revision C.01, M. J. Frisch, G. W. Trucks, H. B. Schlegel, G. E. Scuseria, M. A. Robb, J. R. Cheeseman, G. Scalmani, V. Barone, G. A. Petersson, H. Nakatsuji, X. Li, M. Caricato, A. Marenich, J. Bloino, B. G. Janesko, R. Gomperts, B. Mennucci, H. P. Hratchian, J. V. Ortiz, A. F. Izmaylov, J. L. Sonnenberg, D. Williams-Young, F. Ding, F. Lipparini, F. Egidi, J. Goings, B. Peng, A. Petrone, T. Henderson, D. Ranasinghe, V. G. Zakrzewski, J. Gao, N. Rega, G. Zheng, W. Liang, M. Hada, M. Ehara, K. Toyota, R. Fukuda, J. Hasegawa, M. Ishida, T. Nakajima, Y. Honda, O. Kitao, H. Nakai, T. Vreven, K. Throssell, J. A. Montgomery, Jr., J. E. Peralta, F. Ogliaro, M. Bearpark, J. J. Heyd, E. Brothers, K. N. Kudin, V. N. Staroverov, T. Keith, R. Kobayashi, J. Normand, K. Raghavachari, A. Rendell, J. C. Burant, S. S. Iyengar, J. Tomasi, M. Cossi, J. M. Millam, M. Klene, C. Adamo, R. Cammi, J. W. Ochterski, R. L. Martin, K. Morokuma, O. Farkas, J. B. Foresman, and D. J. Fox, Gaussian, Inc., Wallingford CT, 2016.

(55) Peng, C. S.; Jones, K. C.; Tokmakoff, A. "Anharmonic Vibrational Modes of Nucleic Acid Bases Revealed by 2D IR Spectroscopy," *J. Am. Chem. Soc.* 133(39), 15650-15660 (2011). https://doi.org/10.1021/ja205636h

(56) Ho, J. J.; Skoff, D. R.; Ghosh, A.; Zanni, M. T. "Structural Characterization of Single-Stranded DNA Monolayers Using Two-Dimensional Sum Frequency Generation Spectroscopy," *J Phys Chem B* 119(33), 10586-10596 (2015). https://doi.org/10.1021/acs.jpcb.5b07078

(57) Hamm, P.; Zanni, M. *Concepts and Methods of 2D Infrared Spectroscopy*; Cambridge University Press, 2011.

(58) Krummel, A. T.; Zanni, M. T. "DNA Vibrational Coupling Revealed with Two-Dimensional Infrared Spectroscopy: Insight into Why Vibrational Spectroscopy Is Sensitive to DNA Structure," *The Journal of Physical Chemistry B* 110(28), 13991-14000 (2006). https://doi.org/10.1021/jp062597w

(59) Lee, C.; Park, K.-H.; Cho, M. "Vibrational dynamics of DNA. I. Vibrational basis modes and couplings," *J. Chem. Phys.* 125(11), 114508 (2006). https://doi.org/10.1063/1.2213257

(60) Choi, J.-H.; Cho, M. "Computational IR spectroscopy of water: OH stretch frequencies, transition dipoles, and intermolecular vibrational coupling constants," *J. Chem. Phys.* 138(17), 174108 (2013). https://doi.org/10.1063/1.4802991

(61) Choi, J.-H.; Ham, S.; Cho, M. "Local Amide I Mode Frequencies and Coupling Constants in Polypeptides," *The Journal of Physical Chemistry B* 107(34), 9132-9138 (2003). https://doi.org/10.1021/jp034835i

(62) Clark, M. L.; Ge, A.; Videla, P. E.; Rudshteyn, B.; Miller, C. J.; Song, J.; Batista, V. S.; Lian, T.; Kubiak, C. P. "CO2 Reduction Catalysts on Gold Electrode Surfaces Influenced by Large Electric Fields," *J Am Chem Soc* 140(50), 17643-17655 (2018). https://doi.org/10.1021/jacs.8b09852

(63) Ge, A.; Rudshteyn, B.; Videla, P. E.; Miller, C. J.; Kubiak, C. P.; Batista, V. S.; Lian, T. "Heterogenized Molecular Catalysts: Vibrational Sum-Frequency Spectroscopic, Electrochemical, and Theoretical Investigations," *Acc Chem Res* 52(5), 1289-1300 (2019). https://doi.org/10.1021/acs.accounts.9b00001

(64) Perets, E. A.; Videla, P. E.; Yan, E. C. Y.; Batista, V. S. "Chiral Inversion of Amino Acids in Antiparallel beta-Sheets at Interfaces Probed by Vibrational Sum Frequency Generation Spectroscopy," *J Phys Chem B* 123(27), 5769-5781 (2019). https://doi.org/10.1021/acs.jpcb.9b04029

(65) Bromley, L.; Videla, P. E.; Cartagena-Brigantty, J. L.; Batista, V. S.; Velarde, L. "Binding and Orientation of Carbamate Pesticides on Silica Surfaces," *The Journal of Physical Chemistry C* 127(17), 8399-8410 (2023). https://doi.org/10.1021/acs.jpcc.3c02312

(66) Wang, H. F.; Velarde, L.; Gan, W.; Fu, L. "Quantitative sum-frequency generation vibrational spectroscopy of molecular surfaces and interfaces: lineshape, polarization, and orientation," *Annu Rev Phys Chem* 66189-216 (2015). https://doi.org/10.1146/annurev-physchem-040214-121322

(67) Zhuang, X.; Miranda, P. B.; Kim, D.; Shen, Y. R. "Mapping molecular orientation and conformation at interfaces by surface nonlinear optics," *Physical Review B* 59(19), 12632-12640 (1999). https://doi.org/10.1103/PhysRevB.59.12632

(68) Case, D. A.; Aktulga, H. M.; Belfon, K.; Ben-Shalom, I.; Brozell, S. R.; Cerutti, D.; Cheatham III, T.; Cisneros, G.; Cruzeiro, V.; Darden, T. *Amber 2021*; University of California Press, 2021.

(69) Horn, H. W.; Swope, W. C.; Pitera, J. W.; Madura, J. D.; Dick, T. J.; Hura, G. L.; Head-Gordon, T. "Development of an improved four-site water model for biomolecular simulations: TIP4P-Ew," *The Journal of Chemical Physics* 120(20), 9665-9678 (2004). https://doi.org/10.1063/1.1683075

(70) Zgarbová, M.; Sponer, J.; Otyepka, M.; Cheatham III, T. E.; Galindo-Murillo, R.; Jurecka, P. J. J. o. c. t.; computation. "Refinement of the sugar–phosphate backbone torsion beta for

AMBER force fields improves the description of Z-and B-DNA," 11(12), 5723-5736 (2015). https://doi.org/10.1021/acs.jctc.5b00716

(71) Darden, T.; York, D.; Pedersen, L. "Particle mesh Ewald: An N·log(N) method for Ewald sums in large systems," *The Journal of Chemical Physics* 98(12), 10089-10092 (1993). https://doi.org/10.1063/1.464397

(72) Ryckaert, J.-P.; Ciccotti, G.; Berendsen, H. J. "Numerical integration of the cartesian equations of motion of a system with constraints: molecular dynamics of n-alkanes," *Journal of Computational Physics* 23(3), 327-341 (1977). https://doi.org/10.1016/0021-9991(77)90098-5

(73) Miyamoto, S.; Kollman, P. A. "Settle: An analytical version of the SHAKE and RATTLE algorithm for rigid water models," *Journal of Computational Chemistry* 13(8), 952-962 (1992). https://doi.org/10.1002/jcc.540130805

(74) Pettersen, E. F.; Goddard, T. D.; Huang, C. C.; Couch, G. S.; Greenblatt, D. M.; Meng, E. C.; Ferrin, T. E. "UCSF Chimera—A visualization system for exploratory research and analysis," *Journal of Computational Chemistry* 25(13), 1605-1612 (2004). https://doi.org/https://doi.org/10.1002/jcc.20084

(75) Michaud-Agrawal, N.; Denning, E. J.; Woolf, T. B.; Beckstein, O. "MDAnalysis: a toolkit for the analysis of molecular dynamics simulations," *Journal of Computational Chemistry* 32(10), 2319-2327 (2011). https://doi.org/10.1002/jcc.21787

(76) Ramasubramani, V.; Dice, B. D.; Harper, E. S.; Spellings, M. P.; Anderson, J. A.; Glotzer, S. C. "freud: A software suite for high throughput analysis of particle simulation data," *Computer Physics Communications* 254107275 (2020). https://doi.org/10.1016/j.cpc.2020.107275

(77) Rycroft, C. *Voro++: A three-dimensional Voronoi cell library in C++*; Lawrence Berkeley National Lab.(LBNL), Berkeley, CA (United States), 2009.